Comparison of Transient Diesel Spray Prediction Between Two Commercially Available Computational Fluid Dynamics Codes

S. L. Nicholson, X. H. Fang, J. Camm and M. H. Davy
Department of Engineering Science, University of Oxford, UK

Abstract

Accurate modelling of the initial transient period of spray development is critical within diesel engines, as it impacts on the amount of vapor penetration and hence the combustion characteristics of the spray. In addition, in multiple injection schemes shorter injections will be mostly, if not totally, within the initial transient period. This paper investigates how two different commercially available computational fluid dynamics (CFD) codes (hereafter noted as Code 1 and Code 2) simulate transient diesel spray atomization, in a non-combusting environment. The case considered for comparison is a single-hole injection of n-dodecane representing the Engine Combustion Network's "Spray A" condition. It was identified that the different break-up models used by the codes (Reitz-Diwakar for Code 1, KH-RT for Code 2) had a significant impact on the transient liquid penetration. From differing initial base setups, Code 1's case was matched as closely as possible to Code 2's case. Despite the nominal equivalence between the two simulations, there existed a discrepancy in liquid length prediction throughout injection between codes. This was caused by differing implementations of the KH-RT model in both codes. Therefore, a new implementation of the KH-RT model was input into Code 1 in order to allow correct matching of the liquid length to experimental data throughout the injection period. Results from the new model are shown and compared to the previous implementation, showing an improved ability to match to experimental data.

Introduction

In order to improve existing diesel technology, a better understanding of the dominant physical and chemical phenomenon in spray combustion is required. Previous studies have been conducted to observe in-cylinder spray evolution, air-fuel mixing processes, spray auto-ignition and flame developments [5] [20] [12]. However, these studies are commonly performed in rather simplified configurations which allow limited usage in engine design and optimization [13]. Therefore, Computational Fluid Dynamics (CFD) becomes a more popular and useful tool to integrate experimental studies with physical diesel combustion processes as well as to be part of industrial design and optimization. Among all modelling processes involved in diesel combustion, spray modelling has always been a key component due to its significant impact of fuel injection processes, which greatly affects combustion and emission characteristics. Spray/air mixing involves several different physical processes e.g. collision, evaporation and turbulent mixing. Interactions between these processes are extremely non-linear which makes transient spray modelling really difficult. On this note, it is essential to develop models that could well predict non-reacting spray transient characteristics before reliably implementing these in reacting studies.

Aimed to facilitate validations of multi-scale engine CFD models, Engine Combustion Network (ECN) Initiative promotes collaborative spray and combustion modelling within the engine community through developing a high-fidelity database [10][13]. The database covers key physical properties discovered in both reacting and non-reacting diesel spray experiments including spray liquid and vapor penetration, flame lift-off length, ignition delays, pressure-rise rate and others. Different diesel fuel surrogates were also tested under engine conditions [4][11]. In this study ECN "Spray A" will be investigated and validated against computational models.

Sprays are widely modelled using the Eulerian-Lagrangian approach. The modelling community has been using different codes and commercial CFD packages along with various models, model constants, and grid sizes to study spray characteristics. Some early modelling work in diesel spray was performed through KIVA-3V engine simulation code using n-heptane as the surrogate fuel [19]. Senecal et al. was able to accurately obtain liquid length, ignition delay and flame lift-off length under different ambient and injection conditions. Later Lucchini et al. [7] performed a series of non-reacting diesel spray simulations to determine the required grid sizes for fuel-air mixture formation processes. The OpenFOAM code was capable of capturing liquid length, vapour penetration and mixture fraction distributions at different distances from the injector. Adaptive local mesh refinement techinique (ALMR) was also impletemented to reduce pre-processing and computational time while preserving the simulation accuracy. Som et al. [22] evaluated the Smagorinsky-based large eddy simulation (LES) in n-heptane spray simulation using CFD program CONVERGE. The results were both comparable to a standard Reynolds averaged (RANS) turbulence model and the ECN data. Some global spray and combustion characteristics were successfully captured by both RANS and LES model with LES being slightly better in predicting the ignition delay. More recently Blomberg et al. [3] investigated n-dodecane split

injections using both LES and RANS through Star-CD. In split injection studies, different temperature, injection conditions were varied to capture transient combustion phenomena 'combustion recession'. Both RANS and LES results show good agreement with ECN data in terms of vapour penetration, ignition delay and lift of length. However, liquid penetration and transient jet behaviour are not presented in the study. Although different approaches were used in above studies, global characteristics from both reacting and non-reacting conditions were well captured. One of the biggest challenges associated with these models is uncertainties caused by grid dependency. A great amount of research work has been conducted to resolve grid dependency of spray modelling while keeping simulation cost effective. Beard et al. extended the conventional Lagrangian-Eulerian approach specifically to diesel spray which improves liquid vapour transport behaviour and the momentum coupling between liquid-gas interactions [2]. Different methods were also proposed to overcome this challenge through new sub-models [15][17] and combined Eulerian-Eulerian and Eulerian-Lagrangian method [23]. Aside from grid dependencies, the definition of spray characteristics such as liquid penetration and vapour penetration can also greatly vary the results of the simulation [21]. Therefore it is crucial to standardize modelling strategies as well as simulation definitions. However, due to the complexity of spray simulations there are limited studies concerning comparison of different codes and definitions. Mulane et al. [8] examined cavitation models using both Fluent and Star-CD. Whereas, Karrholm at al. [9] conducted research on the effect of ambient gas temperature and exhaust gas recirculation on spray as well as combustion characteristics. Two different codes, KIVA-3V and OpenFOAM were implemented, which despite some differences, both successfully captured ignition delay and flame lift-off. Iyenger et al. [6] also compared KIVA-3V with OpenFoam to study non-reacting spray, where capability of both codes in predicting low and high ambient temperature non-reacting diesel spray is examined. More recently Som et al. [21] did a comprehensive comparison between OpenFOAM and CONVERGE for both reacting and non-reacting spray modelling. Some definitions for both codes were proposed to aid standardization of the spray simulation.
Major objectives for this paper are then to continue standardizing modelling approaches and definitions for diesel spray simulations and further the modelling of transient high pressure liquid sprays. In this paper, the simulation of single-hole diesel spray ECN "Spray A"under non-reacting conditions is performed in two commercial codes using a Lagrangian-Eulerian approach with RANS turbulence modelling. The results from these simulations are compared: firstly, where each code has been optimized to the experimental data using typically available sub-models and set-ups; and secondly, with the choice of sub-models, grid and model options matched as closely as is possible to each other. These cases are analysed to understand the sources of discrepancies between the simulation results from each code, and to the corresponding experimental data. Following this study, a new implementation of the KH-RT droplet break-up model is proposed and tested utilizing CodeÂă1. Finally, results from CodeÂă1 with this sub-model deployed are compared to the experimental data, showing an improvement in the ability of this code to predict the transient liquid penetration behaviour, without detriment to the steady state liquid penetration or other macroscopic spray characteristics.

Experimental Validation

The simulations presented were compared to experimental data for validation, in this study data from the Engine Combustion Network (ECN) is used for comparison. The ECN has a high-quality, open dataset used for validating and improving computational models using well characterized spray experiments at engine relevant conditions. For this study the non-combusting, n-dodecane fuelled, spray experiment is used as comparison; the experimental data is taken from a constant volume, quiescent, pre-burn combustion vessel which is used to generate the high temperatures (900K) and pressures (∼6MPa) defined as "Spray A"(Table 1). For more information about the experimental methodology see the experimental setup section of Pickett et al (ref). The main comparison between experimental data and computational simulations will be in the form of the liquid length (LL). The liquid length has two major regimes, the initial transient regime and the steady state. The initial transient regime is defined from this point onwards as the first 0.3ms after start of injection (ASOI), with the liquid length after this point being the steady state liquid length. The measurement techniques used for measuring the experimental liquid length can be found in Pickett et al (ref); in the computational simulations the liquid length is defined as the axial distance encompassing 97% of the total liquid mass, and the vapor length is defined as the furthest cell containing a fuel mass fraction of greater than 0.1%, as per ECN definitions (ref).

Table 1. Spray A Sandia Experiments Conditions

Fuel Surrogate	n-dodecane
Ambient Temperature (K)	900
Ambient Gas Density (kg/m^3)	22.8
Gas Composition	0% O_2
Injection Pressure (bar)	1500
Fuel Injection Temperature (K)	363
Nozzle Diameter (μm)	90
Injection Duration (ms)	1.5
Injection Mass (mg)	3.5

Computational Methodology

Within both codes, a grid dependency study was undertaken in the style presented by Senecal [18], where convergence was sought in key computational parameters such as turbulent

kinetic energy, velocity, turbulent length scales and eddy viscosity; the liquid and vapor lengths were also checked for convergence. In both codes a minimum cell size of 0.25mm was found as the best compromise between accuracy and run time; both the trends seen in both studies and the final result matches those seen by Senecal (ref).

Code 1 Methodology

Within Code 1 the constant, pre-burn combustion volume used by Sandia (ref) is simulated using a generated mesh with spray targeted refinement, this can be seen in fig here. The base cell size is 2mm, with a minimum cell size of 0.25mm as found in the aforementioned grid dependency study. A coupled Lagrangian-Eulerian methodology is used, with the spray droplets being modelled by parcels as defined by Dukowicz (ref). In this study the standard $k-\varepsilon$ RANS model (ref) is used to simulate turbulence. Along with the turbulence modelling, accurate modelling of the droplets is crucial for accurate spray prediction. This study uses the Huh-Gosman atomization model (ref) to simulate the near-nozzle region of the spray. The droplets are injected into the domain with a diameter equal to the diameter of the nozzle, and then atomize. The subsequent droplet breakup is modelled by the Reitz-Diwakar breakup model (ref). Models for droplet drag (ref) and turbulent dispersion (12.2 star man) are used in addition to the models above; these are well described within literature and as such are not described here. The droplets vaporize using a Ranz-Marshall vaporization model, which calculates the rate of change of the droplet mass based on the Nusselt and Sherwood numbers (ref 12.6, 12.7 star man). These models are often used within spray simulations (refs) and within Code 1 provide a good match to the steady state liquid length with minimal tuning requirements.

Code 2 Methodology

For Code 2 Sandia combustion chamber is modelled as a 108mm cubical geometry. An innovative, modified cut-cell Cartesian method is implemented to generate the grid. Previous study has shown that a grid using adaptive mesh refinement (AMR) with minimum cell size 0.25mm for RANS-based spray model can give both reasonable accuracy and runtime [18]. A base grid of 4mm is implemented in all cells with a fixed grid embedding of minimum 0.25mm set near the nozzle region. Four levels of AMR is then employed in velocity field. Again Eulerian-Lagrangian approach is used where the gas phase flow field is modelled using standard $k-\varepsilon$ model with modified constants. For liquid phase, the injection process is modelled using “blob ” method from Reitz and Diwakar [14] which the “parcels ” are injected in the computational domain with a characteristic size equal to the nozzle diameter. Droplet breakup and atomization is modelled using the Kelvin-Helmholtz(KH) and Rayleigh-Taylor(RT) models[1]. Based on No Time Counter (NTC) model, the collision model developed by Schmidt and Rutland is used[16]. NTC includes stochastic sub-sampling of parcels within each drop which significantly reduces computational costs. A droplet evaporation model based on Frossling correlation is implemented. Dynamic drag model is used to accurately determine the drag coefficient. Stochastic dispersion model is implemented to capture the effects of turbulence on droplets. A detailed physical model comparison for both codes can be found in Table 2

Table 2. Modelling Setup for both codes

Model Setup	Code 1	Code 2
Turbulence Model	Standard $k-\varepsilon$	Standard $k-\varepsilon$
Spray Models		
Injection models		Blob
Break up	Reitz-Diwakar	KH-RT
Atomization	Huh-Gosman	KH-RT
Collision		NTC
Drag		Dynamic
Evaporation	Ranz-Marshall	Frossling
Dispersion		Stochastic
Heat Transfer	Ranz-Marshall	Ranz-Marshall
Grid		
Type	Structured	Structured with AMR
Dimensionality	3D	3D
Smallest Grid Size	0.25mm	0.25mm
Time Step	Variable Time Step	Variable Time Step

Breakup Model Comparison

From the initial comparisons between codes the breakup models were considered to be a major cause of the transient differences between each codes predictions. This section will detail the two different breakup models used in each code; these models are taken from literature and implemented differently between the two codes.

Code 1 Breakup Model Reitz-Diwakar

Within Code 1 the Reitz-Diwakar breakup model is used, this simulates the breakup of the droplets in a bag-strip style due to the aerodynamic forces on the droplet. The droplet breakup rate is calculated as follows:

$$\frac{dD_d}{dt} = \frac{-D_d - D_{d,stable}}{\tau} \tag{1}$$

h the stable droplet diameter, $D_{d,stable}$ and the breakup timescale τ being calculated within the model. The two breakup methods of bag and strip compete with each other, and the method that produces the shortest breakup timescale will be used to calculate the breakup rate.

Bag Breakup

For bag breakup to occur the droplet Weber number must exceed a critical value:

$$We_d \equiv \frac{\rho_d U^2 D_d}{2\sigma_d} \geq C_{b1} \tag{2}$$

Where C_{b1} is the critical Weber number and a model coefficient and U is the relative velocity of the droplets with respect to the gas phase. All model coefficients and their values used in these simulations can be found in Table . The stable droplet diameter can be found using Eq. 2 when the droplet Weber number is equal to the critical Weber number:

$$D_{d,stable} = \frac{2C_{b1}\sigma_d}{\rho_d U^2} \tag{3}$$

The corresponding breakup timescale can be calculated as follows:

$$\tau_b = \frac{C_{b2}\rho_d{}^{0.5} D_d{}^{1.5}}{4\sigma_d^{0.5}} \tag{4}$$

Where C_{b2} is another model coefficient. Using this breakup timescale and the stable droplet diameter from Eq 3, Eq 1 can be solved to calculate the bag droplet breakup rate.

Strip Breakup

For strip breakup to occur a different criterion is used:

$$\frac{We_d}{\sqrt{\Re_d}} \geqslant C_{S1} \tag{5}$$

When this criterion is met then stripping breakup can occur. Again, the stable droplet diameter can be calculated when the left and right hand side of Eq. 5 are equal to each other:

$$D_{d,stable} = \frac{4\sigma_d{}^2 C_{s1}^2}{\rho_d U^2 \mu_d} \tag{6}$$

Where C_{s1} is a model coefficient. The stripping breakup timescale can be calculated as follows:

$$\tau_s = \frac{C_{s2}}{2}\left(\frac{\rho_d}{\rho_g}\right)^{0.5}\frac{D_d}{U} \tag{7}$$

With C_{s2} another model coefficient. As before, using this breakup timescale and the stable droplet diameter from Eq. 6, Eq.1 can be solved to calculate the stripping droplet breakup rate.

Table 3. Model coefficients and their values used in Code 1 simulations

C_{b1}	6
C_{b2}	π
C_{s1}	0.5
C_{s2}	20

Code 2 Breakup Model - KH-RT

Within Code 2 the KH-RT breakup model is used, with the breakup of the droplets being split into two regimes. For the near nozzle area the Kelvin-Helmholtz (KH) model is used, which simulates the breakup of the large drops due to surface wave growth causing instabilities on the droplet and hence causing drop breakup. For the child droplets formed by the KH breakup the Rayleigh-Taylor (RT) model is applied; this model simulates the breakup of the child droplets due to the rapid deceleration of the droplets from aerodynamic drag. As with Code 1, the droplet breakup rate is calculated in a similar way as Eq.1:

$$\frac{dr_p}{dt} = \frac{-r_p - r_c}{\tau} \tag{8}$$

With the parent droplet radius (r_p) being considered instead of the droplet diameter (D_d) from Eq.1; the child droplet radius (r_c) is calculated from each model along with the breakup timescale (τ), as before.

Kelvin-Helmholtz Breakup

The KH model predicts the growth rate and wavelength of surface waves on each droplet at the flow conditions (Reitz 87). With this knowledge the child droplet radius and breakup timescale can be calculated. The growth rate and wavelength correspond to the maximum computed surface wave growth rate, as this will cause droplet breakup in the shortest possible time and is hence the critical breakup mechanism. The wavelength (Λ_{KH}) can be calculated as follows:

$$\Lambda_{KH} = 9.02\frac{r_p(1+0.45Z_d{}^{0.5})(1+0.4T^{0.7})}{(1+0.865We^{1.67})^{0.6}} \tag{9}$$

With Z_d being the droplet Ohnesorge number and T the Taylor number, both calculated as:

$$Z_d = \frac{\sqrt{We_d}}{Re_d} \tag{10}$$

$$T = Z_d\sqrt{We_g} \tag{11}$$

With the Weber numbers for droplets (We_d) and gases (We_g) being calculated as in Eq.2. To calculate the maximum surface wave growth rate (Ω_{KH}) the following calculation is performed:

$$\Omega_{KH} = \frac{0.34+0.38We_g^{1.5}}{(1+Z_d)(1+T^{0.6})}\sqrt{\frac{\sigma_d}{\rho_d r_p^3}} \tag{12}$$

When the maximum surface wave growth rate and wavelength have been calculated, the child droplet radius can be found:

$$r_c = B_0\Omega_{KH} \tag{13}$$

With B_0 being a model coefficient. All KH-RT model coefficients and their values used in these simulations can be found in Table 4. Finally, the breakup timescale can be calculated:

$$\tau_{KH} = \frac{3.726B_1 r_p}{\Omega_{KH}\Lambda_{KH}} \tag{14}$$

With B_1 as a model coefficient. The results from Eq.13 and Eq.14 can be used in Eq.8 to calculate the parent droplet breakup rate.

Rayleigh-Taylor Breakup

The RT model simulates the instabilities on the droplet surface due to the aerodynamic drag acting on the droplets. This drag is calculated in the form of an acceleration ($\alpha_R T$), which is then applied to the viscid form of the RT model (Joseph et al. 1999). The drag acceleration is calculated as follows:

$$\frac{3}{8} C_d \frac{\rho_g U^2}{\rho_d r_p} \tag{15}$$

The value for the drag coefficient (C_d) is dependent on the Reynolds number:

$$C_d = \begin{cases} \frac{24}{\Re_d}(1 + \frac{\Re_d^{2/3}}{6}) & \Re < 1000 \\ 0.424 & \Re \geq 1000 \end{cases} \tag{16}$$

As in the KH model described above, the maximum surface wave growth rate (Ω_{RT}) is the critical breakup mechanism. Within the viscid RT model the surface wave growth rate is found from:

$$\omega_{RT} = -k_{rt}^2 (\frac{\mu_d + \mu_g}{\rho_d + \rho_g}) + ... \sqrt{k_{RT} (\frac{\rho_d - \rho_g}{\rho_d + \rho_g}) \alpha - \frac{k_{RT}^3 \sigma_d}{\rho_d + \rho_g} + k_{RT}^4 (\frac{\mu_d + \mu_g}{\rho_d + \rho_g})^2} \tag{17}$$

Where k_{RT} is the wavenumber. The wavenumber that corresponds to the maximum surface wave growth rate is KRT, and is found using a numerical bisection method from Eq.17 within Code 2. This value of K_{RT} is then substituted into Eq. 17, replacing k_{RT}, to find the maximum surface wave growth rate (Ω_{RT}). The wavelength that corresponds to this growth rate is calculated as:

$$\Lambda_{RT} = \frac{2\pi}{K_{RT}} \tag{18}$$

Finally, the child droplet radius and breakup time can be calculated:

$$r_c = B_2 \Omega_{RT} \tag{19}$$

$$\tau_{RT} = \frac{B_3}{\Omega_{RT}} \tag{20}$$

With B_2 and B_3as the RT model coefficients. As with the KH model before, the results from Eq.19 and Eq.20 are used with Eq.8 to calculate the parent droplet breakup rate.

Table 4. Model coefficients and their values used in Code 2 simulations

B_0	6
B_1	π
B_2	0.5
B_3	20

Results

This section presents the comparisons undertaken between the two codes. Initially, both codes will be run in their "baseline"setups. These setups are both tuned to match the experimental steady state liquid length. Next, a direct comparison between the two codes will be shown, when both are using the same breakup model (KH-RT) with identical coefficients being used for both the turbulence model and breakup model. This comparison shows that while the breakup models are identical in name, their implementation is clearly different and a cause for further investigation. As a result, a new implementation of the KH-RT model will be applied within Code 1 and will be compared to Code 2, showing an improvement in overall liquid length matching in Code 1.

Baseline Comparison

As mentioned previously, both codes have been optimized for steady state liquid length. This has been achieved through tuning of the turbulence model constants within each code; the other constants are kept as shown in Table 3 and Table 4 for Code 1 and Code 2 respectively. For both codes the $C_{\varepsilon 1}$ constant from the standard $k-\varepsilon$ turbulence model (ref) is increased from its standard value of 1.44 to 1.52 and 1.58 for Code 1 and 2 respectively; within Code 2 the $C_{\varepsilon 2}$ constant is also increased, from its standard value of 1.92 to 1.96. These constant changes allow for the steady state liquid length matches seen in Figure 1. The steady state liquid lengths for both codes are also compared to the experimental steady state liquid length in Table 5.

Table 5. Simulated and Experimental Liquid Length Means for Baseline Cases

Code 1 R-D Steady State LL	10.13mm
Code 2 KH-RT Steady State LL	9.98 mm
Experimental Steady State LL	10.08±0.34mm

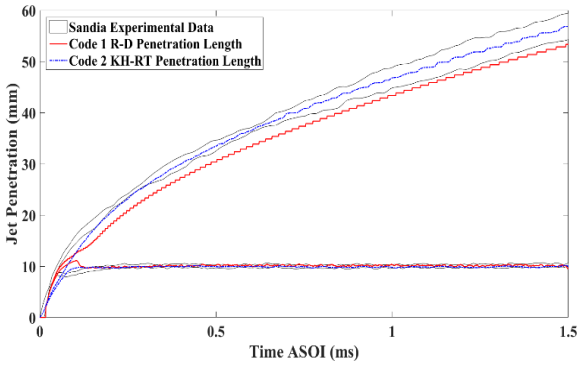

Figure 1. Baseline Simulated and Experimental Liquid and Vapor Lengths against Time ASOI

As shown in Table 5 the two codes both have a very good match to the experimental liquid length; however in Figure 1 it can be

seen the transient prediction is different for each code. Figure 2 shows this transient region in more detail, with a clear overshoot begin seen for Code 1 and Code 2 having a slower initial gradient but a minimal overshoot.

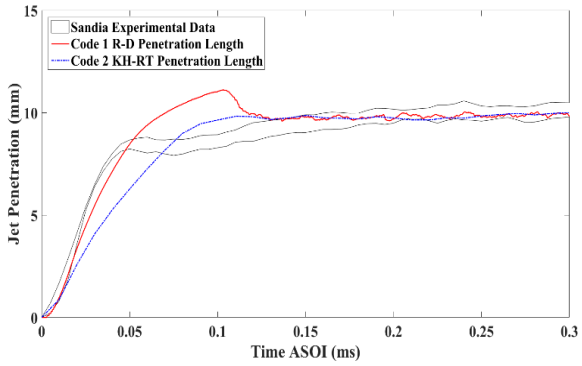

Figure 2. Transient Liquid Length Prediction of Each Code in Baseline Setups

The reason for this transient overshoot can be seen by looking at the movement of the initially injected parcels through the domain. As fig here shows, there is a group of large parcels that move through the spray early in the injection, with their momentum causing them to reach the tip of the spray and penetrate further than the rest of the parcels. Given these parcels are large in diameter they will contain a reasonable mass, and given the definition of liquid length earlier as a percentage of the total liquid mass in the system, when they overshoot the liquid tip they cause the overshoot seen in the liquid length shown in Figure 2. These large parcels are not seen in Code 2's simulation, suggesting that the difference in breakup model could be the cause of the difference in transient prediction between the two codes. As a result, the next comparison will be a more direct one, with Code 1's setup being changed to match as closely as possible that of Code 2. This will offer further insight into whether the breakup model is causing the initial overshoot.

Direct Comparison

Now, Code 1 is matched to Code 2's Spray A setup, altering the $k-\varepsilon$ turbulence model constants and using the KH-RT model with the constants set to those shown in Table 4. This will offer a direct comparison between the codes on their utilization of the same models. The spray penetration results can be seen in Figure 3.

droplet flag will show whether the droplet has undergone breakup beforehand, and as such the KH-RT implementation will be closer to that of Code 2. Also, comparisons will be made to new experimental data from the shock tube (ref), this experimental data will go to higher temperatures and pressures than seen in the Spray A condition and will be used to test breakup models more stringently (reword).

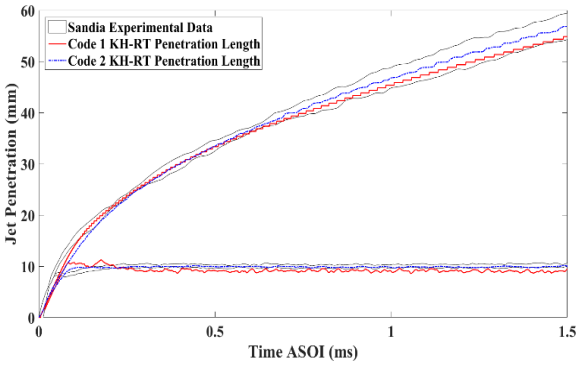

Figure 3. Direct Comparison of Code 1 and Code 2 Penetration Lengths against Experimental Data Over Time ASOI

The results from Figure 3 show that there is a difference in prediction of the liquid lengths between the two codes, with Code 1 initially over-predicting, then under-predicting the liquid length. Within the initial transient period the liquid length is over-predicted, this is shown in Figure 4.

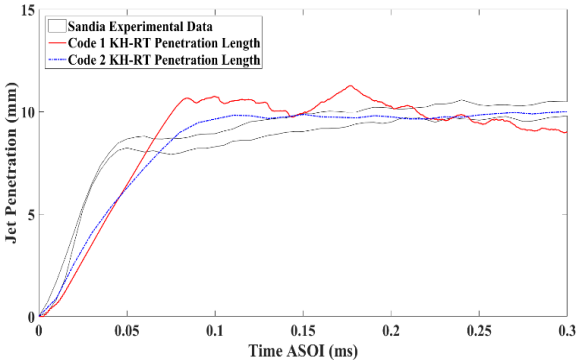

Figure 4. Transient Comparison of Code 1 and Code 2's Simulation of Liquid Length against Experimental Data Over Time ASOI

The steady state liquid length is shown in Table 4; when compared to the previous simulation in Code 1 it is clearly under-predicting the steady state liquid length whilst not capturing the transient prediction of Code 2 and is in fact outside of the experimental steady state liquid length range. This difference in prediction can be explained by differences in the implementation of the KH-RT model between codes.

Table 6. Simulated and Experimental Steady State Liquid Length Means for Baseline and KH-RT Comparison Cases

Code 1 R-D Steady State LL	10.13mm
Code 1 KH-RT Steady State LL	10.13mm
Code 2 KH-RT Steady State LL	9.98 mm
Experimental Steady State LL	10.08±0.34mm

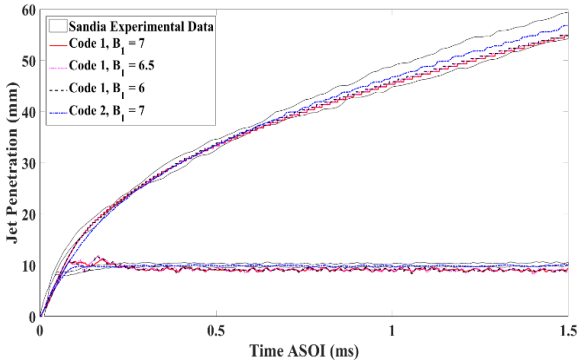

Figure 6. Penetration Lengths for Varying B_1 Values against Time ASOI

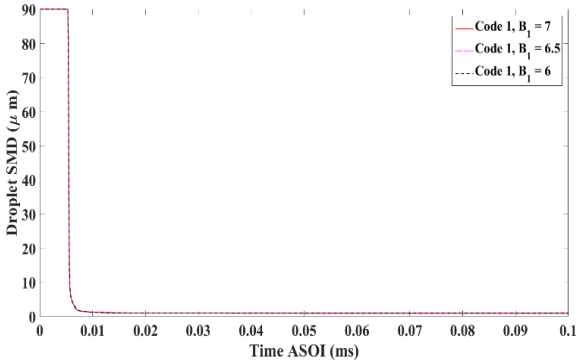

Figure 7. Global SMD Values for VaryingB_1 Values against Time ASOI

KH-RT Implementation Differences

Between Code 1 and Code 2 the KH-RT model utilizes the same equations, however the implementation of the relationship between the KH and RT models is different. Whilst Code 2 implements the RT model only on child droplets (droplets that have already undergone a breakup, in this case using the KH model), within Code 1 the KH and RT models compete (as with the Reitz-Diwakar model), with the shortest breakup timescale calculated causing breakup. As a result there is an expectation of a difference in results between supposedly identical models, as shown in Figure 3 and Figure 4. This difference can be seen more clearly by looking at the global Sauter Mean Diameter (SMD) numbers, as shown in Figure 5.

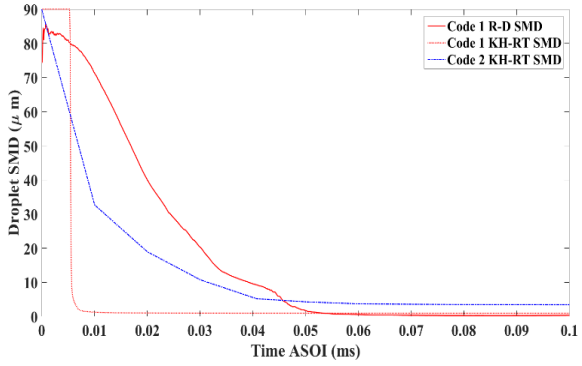

Figure 5. Global SMD Values for Baseline Cases for Code 1 and Code 2, and KH-RT Case for Code 1 against Time ASOI

The parcel plots shown in fig here illustrate this difference very clearly, with Code 1 showing a rapid breakup of nozzle diameter droplets to a large amount of very small droplets, very quickly after injection. This rapid breakup correlates well with just the RT model causing breakup, as a stripping breakup model will cause many very small droplets to be formed after breakup. This suggests that within Code 1 the RT model is dominating breakup, even within the liquid core.

A further test for the Code 1 version of the KH-RT model is undertaken by lowering the B1 constant from Eq.14. Figure 6 and Figure 7 show that this can be seen to have minimal impact on either the liquid and vapor lengths or SMD numbers, suggesting that even with a shorter timescale for KH breakup the RT breakup timescale is shorter still and dominating breakup. This is not what one would expect physically as the liquid core will be a low drag region of the spray and as such any stripping breakup will be minimal and should be dominated by surface wave growth. As a result, a new implementaoxford.gov.uktion of the KH-RT model within Code 1 is required to stop this behavior from being simulated. Currently within Code 1 there is no flag for child droplets as is seen in Code 2, as a result a “breakup length” model will be implemented within Code 1.

Breakup Length Model Implementation

For the breakup length model a user defined function (UDF) was input into Code 1, utilizing the governing equations of the KH-RT model (Eq.18-Eq. 20) (ref) and converting all radii to diameters for use with Code 1’s droplet breakup rate equation (Eq.1). A breakup length criterion is added to the model, which is used to define when the “switch”of the two breakup models takes place; before the breakup length is reached only the KH breakup model acts and after droplets pass the breakup length both the KH and RT breakup models are used. The model coefficients are kept the same as before (shown in Table 4) so as

to keep the simulations as consistent as possible between model implementations. The breakup length is calculated as follows:

$$L_b = C_{bl}\sqrt{\frac{\rho_l}{\rho_g}}D_0 \tag{21}$$

Where D_0 is the nozzle diameter and C_{bl} a tunable breakup length coefficient. Details of the impact of the Cbl coefficient are presented, and an optimum value is found. It should also be noted that setting C_{bl} to zero will result in the initial Code 1 methodology applying to droplet breakup, as seen in Patterson (ref Patterson 97). oxford.gov.uk

Final Comparison

Conclusions

Within this study baseline comparisons have been made between two codes at setups optimized for steady state liquid lengths. Differences in transient predictions have been observed between the codes, with the breakup model considered the cause of the differences. A direct comparison between codes has shown a difference in implementation between seemingly identical models, leading to a difference in overall liquid length prediction between codes. A new implementation of the KH-RT model has been used within Code 1, allowing for the two models to act at different regions of the spray. This implementation shows

Future Work

A further improvement on the implementation of the KH-RT model within Code 1 will be applied, based on a new droplet flag. This droplet flag will show whether the droplet has undergone breakup beforehand, and as such the KH-RT implementation will be closer to that of Code 2. Also, comparisons will be made to new experimental data from the shock tube (ref), this experimental data will go to higher temperatures and pressures than seen in the Spray A condition and will be used to test breakup models more stringently (reword)

References

[1] J. C. Beale and R. D. Reitz. Modeling spray atomization with the kelvin-helmholtz/rayleigh-taylor hybrid model. *Atomization and sprays*, 9(6), 1999.

[2] P. Beard, J.-M. Duclos, C. Habchi, G. Bruneaux, K. Mokaddem, and T. Baritaud. Extension of lagrangian-eulerian spray modeling: Application to high pressure evaporating diesel sprays. In *SAE Technical Paper*. SAE International, 06 2000.

[3] Blomberg, C., Zeugin, L., Pandurangi, S., Bolla, M. et al. Modeling Split Injections of ECN Spray A Using a Conditional Moment Closure Combustion Model with RANS and LES. *SAE Int. J. Engines*, 9(4), January 2016.

[4] G. D'Errico, D. Ettorre, and T. Lucchini. Simplified and detailed chemistry modeling of constant-volume diesel combustion experiments. *SAE International Journal of Fuels and Lubricants*, 1(1):452–465, apr 2008.

[5] A. W. H.J. Koss and H. Baeker. Spray propagation, mixture formation, autoignition and soot formation of multi-component fuels in pressure chamber. *Technical Report*, 1993.

[6] S. V. Iyengar, C.-W. Tsang, and C. Rutland. Validating non-reacting spray cases with kiva-3v and openfoam. In *SAE Technical Paper*. SAE International, 04 2013.

[7] T. Lucchini, G. D. Errico, D. Ettorre, and G. Ferrari. Numerical investigation of non-reacting and reacting diesel sprays in constant-volume vessels. *SAE Int. J. Fuels Lubr.*, 2:966–975, 06 2009.

[8] A. Mulemane, S. Subramaniyam, P.-H. Lu, J.-S. Han, M.-C. Lai, and R. Poola. Comparing cavitation in diesel injectors based on different modeling approaches. In *SAE 2004 World Congress and Exhibition*. SAE International, mar 2004.

[9] F. Peng Karrholm, F. Tao, and N. Nordin. Three-dimensional simulation of diesel spray ignition and flame lift-off using openfoam and kiva-3v cfd codes. In *SAE World Congress and Exhibition*. SAE International, apr 2008.

[10] L. M. Pickett. Introducing the engine combustion network. In *International Multidimensional Engine Modeling Users Group Meeting*, 2008.

[11] L. M. Pickett and J. Abraham. Computed and measured fuel vapor distribution in a diesel spray. *Atomization and Sprays*, 20(3):241–250, 2010.

[12] L. M. Pickett, C. L. Genzale, G. Bruneaux, L.-M. Malbec, L. Hermant, C. Christiansen, and J. Schramm. Comparison of diesel spray combustion in different high-temperature, high-pressure facilities. *SAE International Journal of Engines*, 3(2):156–181, oct 2010.

[13] L. M. Pickett, C. L. Genzale, G. Bruneaux, L.-M. Malbec, L. Hermant, C. Christiansen, and J. Schramm. Comparison of diesel spray combustion in different high-temperature, high-pressure facilities. *SAE International Journal of Engines*, 3(2):156–181, oct 2010.

[14] R. D. Reitz and R. Diwakar. Structure of high-pressure fuel sprays. In *SAE International Congress and Exposition*. SAE International, feb 1987.

[15] D. P. Schmidt and C. Rutland. A new droplet collision algorithm. *Journal of Computational Physics*, 164(1):62 – 80, 2000.

[16] D. P. Schmidt and C. Rutland. A new droplet collision algorithm. *Journal of Computational Physics*, 164(1):62 – 80, 2000.

[17] D. P. Schmidt and P. K. Senecal. Improving the numerical accuracy of spray simulations. In *SAE Technical Paper*. SAE International, 03 2002.

[18] P. Senecal, E. Pomraning, K. Richards, and S. Som. Grid convergent spray models for internal combustion engine cfd simulations. page 14. American Society of Mechanical Engineers, American Society of Mechanical Engineers, 20120923 2012.

[19] P. K. Senecal, E. Pomraning, K. J. Richards, T. E. Briggs, C. Y. Choi, R. M. McDavid, and M. A. Patterson. Multi-dimensional modeling of direct-injection diesel spray liquid length and flame lift-off length using cfd and parallel detailed chemistry. In *SAE Technical Paper*. SAE International, 03 2003.

[20] D. L. Siebers and B. Higgins. Flame lift-off on direct-injection diesel sprays under quiescent conditions. In *SAE 2001 World Congress*. SAE International, mar 2001.

[21] S. Som, G. D'Errico, D. Longman, and T. Lucchini. Comparison and standardization of numerical approaches for the prediction of non-reacting and reacting diesel sprays. In *SAE Technical Paper*. SAE International, 04 2012.

[22] S. Som, P. Senecal, and E. Pomraning. Comparison of rans and les turbulence models against constant volume diesel experiments. In *24th Annual Conference on Liquid Atomization and Spray Systems, ILASS Americas, San Antonio, TX*, 2012.

[23] A. Vallet, A. A. Burluka, and R. Borghi. Development of a eulerian model for the atomization of a liquid jet. *Atomization and Sprays*, 11(6), 2001.